

# Magnetic and luminescent properties of multifunctional $\text{GdF}_3:\text{Eu}^{3+}$ nanoparticles

Hon-Tung Wong, H. L. W. Chan, and J. H. Hao<sup>a)</sup>

Department of Applied Physics and Materials Research Centre, The Hong Kong Polytechnic University, Hung Hom, Hong Kong, People's Republic of China

(Received 15 April 2009; accepted 15 June 2009; published online 14 July 2009)

Multifunctional  $\text{GdF}_3:\text{Eu}^{3+}$  nanoparticles were synthesized using a hydrothermal method. Photoluminescent excitation and emission spectra, and lifetime were measured. The average lifetime of the nanoparticles is about 11 ms. The nanoparticle exhibits paramagnetism at both 293 and 77 K, ascribing to noninteracting localized nature of the magnetic moment in the compound. The magnetic properties of  $\text{GdF}_3:\text{Eu}^{3+}$  is intrinsic to the  $\text{Gd}^{3+}$  ions, which is unaffected by the doping concentration of the  $\text{Eu}^{3+}$  luminescent centers. A measured magnetization of approximately 2 emu/g is close to reported values of other nanoparticles for bioseparation. © 2009 American Institute of Physics. [DOI: 10.1063/1.3177194]

Rare earth (RE) fluoride was found to be a promising host lattice due to its low phonon energy leading to a minimization of quenching of the excited states. This gives rise to a long luminescent lifetime and high luminescent quantum yields.<sup>1</sup> Moreover, the ease of substitution of the RE ions by other doping RE ions with the same valence, and the small particles size of the RE fluoride make it appealing to biological applications.<sup>1-3</sup> Magnetic properties of these RE fluoride nanoparticles are crucial to their uses in some biological applications such as bioseparation and magnetic resonance imaging (MRI). However, hitherto, studies on the RE fluoride nanoparticles mainly focus on morphology control, synthesis conditions, luminescent properties, and biocompatibility.<sup>4-6</sup> There is little study of the physical mechanisms responsible for their physical properties. A recent report utilizing  $\text{GdF}_3$  nanoparticle as a contrast agent for MRI application gave promising results due to its high solubility in a range of solvents, high mass relaxivity (i.e., short water-proton relaxation time in MRI), and ease of surface modifications for specific imaging needs.<sup>7</sup> However, only relaxation rates were given without detailed characterization of its magnetic properties. The dependences of its magnetization on temperature and applied field were unknown, especially for fluoride nanoparticles with intrinsic luminescent and magnetic properties. In this letter, detailed physical mechanisms elucidating the intrinsic luminescent and magnetic properties of the multifunctional  $\text{GdF}_3:\text{Eu}^{3+}$  nanoparticle are reported. The dependences of the magnetization on temperature and applied field are determined.

$\text{GdF}_3: 5\% \text{Eu}^{3+}$  nanoparticles were prepared using hydrothermal synthesis.  $\text{Gd}(\text{NO}_3)_3$ ,  $\text{Eu}(\text{NO}_3)_3$  solutions, and NaF particles were mixed in de-ionized (DI) water under magnetic stirring. After the NaF was dissolved, the colloidal solution was then transferred to a tightly capped beaker at 80 °C for 2 h under magnetic stirring in air. The colloidal solution was then transferred to a hydrothermal autoclave and hydrothermally treated at 180 °C under a pressure of about 700 kPa for 18 h. The obtained particle was then sepa-

rated and cleaned by centrifugation using DI water for three times, and dried at 80 °C for 12 h in air.

Figure 1 shows an x-ray diffraction (XRD) pattern of the  $\text{GdF}_3: 5\% \text{Eu}^{3+}$  nanoparticles. The diffraction pattern is in good agreement with a JCPDS standard card<sup>8</sup> of an orthorhombic  $\text{GdF}_3$  crystal phase and space group  $Pnma$ , which also agrees with that reported in the literature.<sup>6</sup> The obtained nanoparticles are mainly composed of elongated nanoparticles, with a small proportion of spherical and nearly spherical nanoparticles. The average length and width of the elongated nanoparticles are around 100 and 50 nm, respectively; while the average sizes of the spherical and nearly spherical nanoparticles are around 40 nm.

Room-temperature photoluminescent excitation (PLE) (monitored at 592 nm of  $\text{Eu}^{3+}: ^5D_0 \rightarrow ^7F_1$ ) and emission (PL; excited at 394 nm of  $\text{Eu}^{3+}: ^7F_0 \rightarrow ^5L_6$ ) spectra of the  $\text{GdF}_3: 5\% \text{Eu}^{3+}$  nanoparticles are shown in Figs. 2(a) and 2(b), respectively. The excitation peaks at 361, 378, and 394 nm originate from the excitations from the ground states of  $^7F_0$  to various excited states of the  $\text{Eu}^{3+}$  ions; while other excitation peaks at 273 and 311 nm originate from the transitions of the  $\text{Gd}^{3+}$  ions, respectively. As the intensity of the prominent excitation peak of the  $\text{Gd}^{3+}$  ions at 273 nm is comparable to that of the  $\text{Eu}^{3+}$  ions at 394 nm, there exists an efficient energy transfer from the  $\text{Gd}^{3+}$  ions to the  $\text{Eu}^{3+}$  ions. Thus, the pattern of the PL spectrum excited at 273 nm is identical to that excited at 394 nm. A series of characteristics

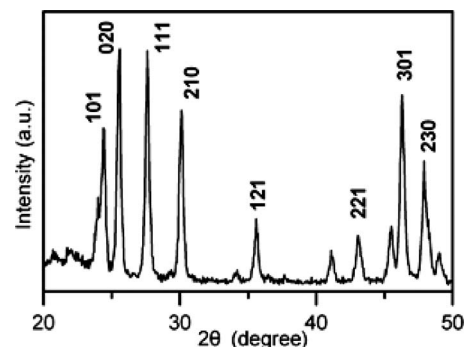


FIG. 1. XRD pattern of the  $\text{GdF}_3: 5\% \text{Eu}^{3+}$  nanoparticle with dominant peaks labeled.

<sup>a)</sup> Author to whom correspondence should be addressed. Electronic mail: apjhao@polyu.edu.hk.

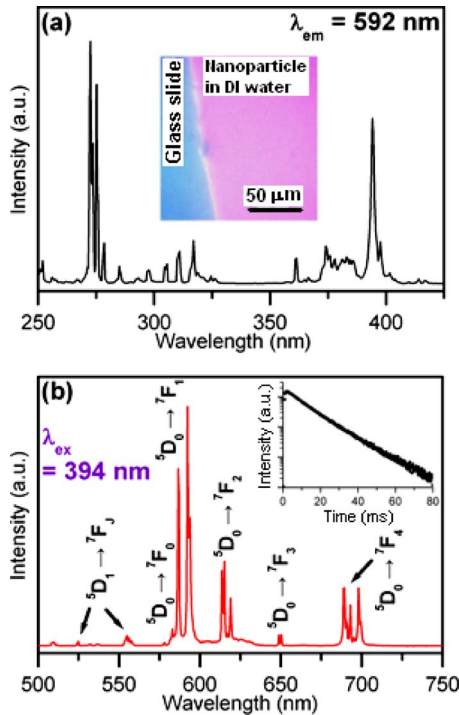


FIG. 2. (Color online) (a) PLE and (b) PL spectra of the  $\text{GdF}_3: 5\% \text{Eu}^{3+}$  nanoparticle. Inset in (a) is the fluorescent microscopy image of the  $\text{GdF}_3: 5\% \text{Eu}^{3+}$  nanoparticles in DI water (right part) under UV excitation taken at the edge of the droplet. Inset in (b) is the luminescent decay profile for emission at 592 nm.

emission lines of the  $\text{Eu}^{3+}$  ions ranging from 500 to 750 nm is clearly observed in Fig. 2(b), corresponding to the radiative transitions from the excited  $^5D_1$  and  $^5D_0$  to the  $^7F_J$  with the  $^5D_0 \rightarrow ^7F_1$  orange emission as the most prominent one. It is well known that the crystal site symmetry of the doping  $\text{Eu}^{3+}$  ions affects the relative intensities of  $^5D_0 \rightarrow ^7F_1$  and  $^5D_0 \rightarrow ^7F_2$  transitions. As the doping  $\text{Eu}^{3+}$  ions occupy the  $\text{Gd}^{3+}$  ions lattice sites and are at the sites with inversion symmetry, the  $^5D_0 \rightarrow ^7F_1$  magnetic-dipole transition is dominant; and the  $^5D_0 \rightarrow ^7F_2$  electric-dipole transition is forbidden under this inversion symmetry which decreases in intensity.<sup>3,6</sup> The existence of the  $^5D_1 \rightarrow ^7F_J$  transitions from the higher  $\text{Eu}^{3+}$  energy level is due to the inefficient energy transfer between the  $\text{Eu}^{3+}$  ions at this low  $\text{Eu}^{3+}$  doping level ( $\text{GdF}_3: 5\% \text{Eu}^{3+}$ ), which is consistent with the results reported previously.<sup>9</sup>

The nanoparticles were dispersed in DI water under ultrasonic treatment. The corresponding fluorescent microscopy image under UV excitation is shown in the inset of Fig. 2(a). A red emission is clearly observed, which suggests that the emission intensity of the nanoparticles is adequate for vision in biological applications, e.g., in labeling of cells. The inset of Fig. 2(b) shows a luminescent decay of the 592 nm emission (excited at 394 nm) with biexponential nature, suggesting the presence of two luminescent decay centers with different probabilities of nonradiative decay.<sup>3,10</sup> Using the formula for average lifetime  $\langle \tau \rangle = (A_1 \tau_1^2 + A_2 \tau_2^2) / (A_1 \tau_1 + A_2 \tau_2)$ ,<sup>11</sup>  $\langle \tau \rangle$  is determined to be 11.0 ms. When the excitation wavelength is changed to 273 nm with all other conditions remained the same, the same biexponential nature and average lifetime of 11.2 ms are obtained, ascribing to the efficient energy transfer in  $\text{Gd}^{3+}$  to  $\text{Eu}^{3+}$  ions. The average lifetime of the  $\text{GdF}_3: 5\% \text{Eu}^{3+}$  nanoparticles ( $\sim 11$  ms) is

TABLE I. Fitting curve and parameters for the luminescent decay (emission at 592 nm) at excitation wavelengths of 394 and 273 nm. Fitting curve:  $I = A_1 \exp(-t/\tau_1) + A_2 \exp(-t/\tau_2)$ .

Excitation wavelength (nm)	394	273
$A_1$	18 763.26	92 909.24
$\tau_1$ (ms)	9.68	9.88
$A_2$	464.07	961.94
$\tau_2$ (ms)	28.60	41.51
$\langle \tau \rangle$ (ms)	11.0	11.2

longer than that reported for the  $\text{Gd}_2\text{O}_3: 5\% \text{Eu}^{3+}$  nanoparticle ( $\sim 2$  ms), resulting from the lower phonon energy in the fluoride host compared to the oxide. The fitting curve and calculated parameters are shown in Table I.

The existence of ferromagnetism of the Gd atom below 289 K motivates us to investigate the magnetic properties of the multifunctional  $\text{GdF}_3: 5\% \text{Eu}^{3+}$  nanoparticles, and magnetization as a function of applied magnetic field measured using a vibrating sample magnetometer at 293 and 77 K is shown in Fig. 3. The nanoparticles at both 293 K (applied field range from  $-20$  to  $20$  kOe) and 77 K (applied field range from  $-15$  to  $15$  kOe) show paramagnetism, unlike the behavior of Gd atoms. The magnetic properties of the  $\text{Gd}^{3+}$  ions come from seven unpaired inner  $4f$  electrons, which are closely bound to the nucleus and effectively shielded by the outer closed shell electrons  $5s^2 5p^6$  from crystal field. When the  $\text{Gd}^{3+}$  ions react with  $\text{F}^-$  ions to form  $\text{GdF}_3$ , the separation between the  $\text{Gd}^{3+}$  ions in the  $\text{GdF}_3$  matrix are too far away. Thus, it inhibits sufficient overlap of the orbitals associated with the partially filled  $4f$  electrons shells of the  $\text{Gd}^{3+}$  ions necessary for ferromagnetism. It turns out that the magnetic moments associated with the  $\text{Gd}^{3+}$  ions are all localized and noninteracting giving rise to paramagnetism.<sup>12,13</sup> Therefore, the  $\text{GdF}_3: \text{Eu}^{3+}$  nanoparticles show paramagnetism even at 77 K, unlike the Gd atom showing ferromagnetism at low temperature.

The magnetic mass susceptibility of the  $\text{GdF}_3: 5\% \text{Eu}^{3+}$  nanoparticles at 293 and 77 K are found to be  $0.94 \times 10^{-4}$  and  $4.07 \times 10^{-4}$  emu/g Oe, respectively. An increase in the magnetic susceptibility at low temperature (77 K) is due to the reduction in thermal fluctuation, which is a typical behavior in paramagnetic materials described by the Curie's law. The magnetic susceptibility of our nanoparticles at 293 K is comparable to that of the  $\text{Gd}_2\text{O}_3: \text{Eu}^{3+}$  nanoparticles reported in the literature, which again verify the noninteracting localized nature of the magnetic moment.<sup>14</sup>

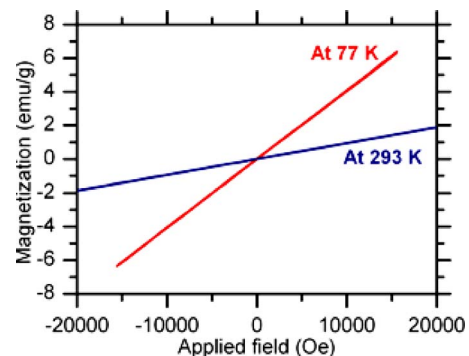


FIG. 3. (Color online) Magnetization vs magnetic field of the  $\text{GdF}_3: 5\% \text{Eu}^{3+}$  nanoparticles at 293 and 77 K.

Nanoparticles for bioseparation reported in the literature are mainly superparamagnetic with many different structures, such as magnetic core/luminescent shell assembly, and magnetic-luminescent nanoparticles embedded silica nanocomposites. Among these structures, iron oxides are usually employed for the functional magnetic units with the minimum saturation magnetization reported to be about 3.2 emu/g.<sup>15</sup> Iron oxides are superparamagnetic, however, there is no intrinsic luminescent properties. The magnetic properties of the nanoparticles employing iron oxides are reported to be deteriorated by the outer luminescent shells to a certain extent.<sup>16,17</sup> In contrast to the iron oxides, the GdF<sub>3</sub>:5% Eu<sup>3+</sup> nanoparticles exhibit both intrinsic luminescent and magnetic properties. In our experiments, the magnetic properties of the GdF<sub>3</sub>:Eu<sup>3+</sup> nanoparticles are intrinsic to the Gd<sup>3+</sup> ions, which is found to be unaffected by the doping concentration of the Eu<sup>3+</sup> luminescent centers. Although the nanoparticles only exhibit paramagnetism, the magnetization at 20 kOe (at 293 K) is around 2 emu/g, which is near to the reported value of the nanoparticles used for common bioseparation.<sup>15</sup> Besides, the emission intensity of the GdF<sub>3</sub>:5% Eu<sup>3+</sup> nanoparticle in DI water is adequate for visual inspection as shown in the inset of Fig. 2(a). Therefore, the GdF<sub>3</sub>:5% Eu<sup>3+</sup> nanoparticles may find uses in bioseparation in terms of the closeness in magnetization to reported values and adequate emission intensity in aqueous solutions.

In conclusion, the GdF<sub>3</sub>:Eu<sup>3+</sup> nanoparticles exhibit paramagnetism ascribing to the insufficient overlap of orbitals associated with unpaired 4*f* electrons shells. Our measurements indicate possibilities of our nanoparticles as biolabels for bioseparation and MRI.

The work was supported by a grant from the Hong Kong Polytechnic University (Grant No. J-BB9R). We acknow-

ledge Mr. Kai To Lai and Mr. Zhou Xu for their help in the synthesis of the nanoparticles, and Mr. Ting Su for the capture of the fluorescent microscopy image.

- <sup>1</sup>Z. L. Wang, H. L. W. Chan, H. L. Li, and J. H. Hao, *Appl. Phys. Lett.* **93**, 141106 (2008).
- <sup>2</sup>M. Nyk, R. Kumar, T. Y. Ohulchanskyy, E. J. Bergey, and P. N. Prasad, *Nano Lett.* **8**, 3834 (2008).
- <sup>3</sup>D. Q. Chen, Y. S. Wang, Y. L. Yu, and P. Huang, *J. Phys. Chem. C* **112**, 18943 (2008).
- <sup>4</sup>Z. G. Chen, H. L. Chen, H. Hu, M. X. Yu, F. Y. Li, Q. Zhang, Z. G. Zhou, T. Yi, and C. H. Huang, *J. Am. Chem. Soc.* **130**, 3023 (2008).
- <sup>5</sup>R. T. Wegh, H. Donker, K. D. Oskam, and A. Meijerink, *Science* **283**, 663 (1999).
- <sup>6</sup>C. X. Li, J. Yang, P. P. Yang, H. Z. Lian, and J. Lin, *Chem. Mater.* **20**, 4317 (2008).
- <sup>7</sup>F. Evancics, P. R. Diamente, F. C. J. M. van Veggel, G. J. Stanisiz, and R. S. Prosser, *Chem. Mater.* **18**, 2499 (2006).
- <sup>8</sup>JCPDS Card No. 12-0788.
- <sup>9</sup>X. P. Fan, D. B. Pi, F. Wang, J. R. Qiu, and M. Q. Wang, *IEEE Trans. Nanotechnol.* **5**, 123 (2006).
- <sup>10</sup>J. H. Hao, S. A. Studenikin, and M. Cocivera, *J. Appl. Phys.* **90**, 5064 (2001).
- <sup>11</sup>Z. L. Wang, G. Z. Li, Z. W. Quan, D. Y. Kong, X. M. Liu, M. Yu, and J. Lin, *J. Nanosci. Nanotechnol.* **7**, 602 (2007).
- <sup>12</sup>D. Jiles, *Introduction to Magnetism and Magnetic Materials*, 2nd ed. (Chapman and Hall, London, 1998), Chaps. 9, 11.
- <sup>13</sup>J. R. Christman, *Fundamentals of Solid State Physics* (Wiley, New York, 1988), Chap. 11.
- <sup>14</sup>L. G. Jacobsohn, B. L. Bennett, R. E. Muenchausen, S. C. Tornga, J. D. Thompson, O. Ugurlu, D. W. Cooke, and A. L. L. Sharma, *J. Appl. Phys.* **103**, 104303 (2008).
- <sup>15</sup>H. H. Yang, S. Q. Zhang, X. L. Chen, Z. X. Zhuang, J. G. Xu, and X. R. Wang, *Anal. Chem.* **76**, 1316 (2004).
- <sup>16</sup>H. C. Lu, G. S. Yi, S. Y. Zhao, D. P. Chen, L. H. Guo, and J. Cheng, *J. Mater. Chem.* **14**, 1336 (2004).
- <sup>17</sup>D. Dosev, M. Nichkova, R. K. Dumas, S. J. Gee, B. D. Hammock, K. Liu, and I. M. Kennedy, *Nanotechnology* **18**, 055102 (2007).